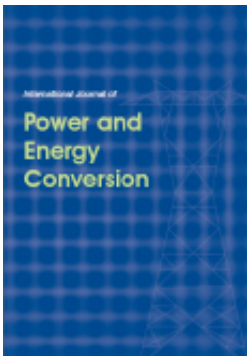

International Journal of Power and Energy Conversion

ISSN online: 1757-1162 - ISSN print: 1757-1154
https://www.inderscience.com/ijpec

Evaluation of radiation protection properties of novel concrete mixture against photon energy in nuclear applications: simulation and experimental findings

Brahim El Azzaoui, Mohamed Youssef Messous, Abdessamad Didi, El Mahjoub Chakir, El Mehdi Alibrahmi

DOI: 10.1504/IJPEC.2023.10060927

Article History:

Received:	18 July 2023
Last revised:	27 September 2023
Accepted:	27 September 2023
Published online:	14 December 2023

Evaluation of radiation protection properties of novel concrete mixture against photon energy in nuclear applications: simulation and experimental findings

Brahim El Azzaoui*

LPMS, Faculty of Sciences,
Ibn Tofail University,
Kenitra, Morocco
and
DSS/DPTS/URP/National Center for Nuclear Energy,
Science and Technology,
Rabat, Morocco
Email: brahim.elazzaoui1@uit.ac.ma
*Corresponding author

Mohamed Youssef Messous and Abdessamad Didi

National Center for Nuclear Energy, Science and Technology,
Rabat, Morocco
Email: messous@cnesten.org.ma
Email: ijpec.didi@gmail.com

El Mahjoub Chakir and El Mehdi Alibrahmi

LPMS, Faculty of Sciences,
Ibn Tofail University,
Kenitra, Morocco
Email: elmahjoub.chakir@uit.ac.ma
Email: alibrahimi.elmehdi@uit.ac.ma

Abstract: This study aims to develop highly effective radiation shielding materials for nuclear applications. It investigates concrete mixtures containing barite from five ore sites in Southeast Morocco, emphasising their gamma and X-ray shielding capabilities. Simulations compare four mixtures from each site. Samples with superior radiation attenuation are experimentally tested for validation of the results obtained by MCNP, DOSIMEX, and XCOM. The study reveals a concrete blend (16% cement, 69% Agdz ore barite, 5% sand, and 10% water) as an excellent radiation shield. The Agdz site, with 57.48% barite content, proves the most effective. Good agreement between calculated and empirical data highlights the research's reliability. Dose rate investigations show a 6% average gap between MCNP and DOSIMEX and a 9% difference between DOSIMEX and experiments.

Keywords: attenuation; concrete mixtures; barite; radiation shielding; radiation protection.

Reference to this paper should be made as follows: El Azzaoui, B., Messous, M.Y., Didi, A., Chakir, E.M. and Alibrahmi, E.M. (2023) 'Evaluation of radiation protection properties of novel concrete mixture against photon energy in nuclear applications: simulation and experimental findings', *Int. J. Power and Energy Conversion*, Vol. 14, No. 4, pp.376–392.

Biographical notes: Brahim El Azzaoui is a PhD student at Ibn Tofail University, Faculty of Sciences at Kenitra, specialises in the development of innovative shielding materials designed to attenuate ionising radiation, including Gamma rays, X-rays, and neutrons. With an extensive background encompassing over 12 years of practical experience, he has served as in charge of Radiation Protection at the National Center for Nuclear Energy, Science, and Technology. His expertise includes ensuring compliance with shielding standards, occupational radiation protection at research reactors, radiological risk assessment, and conducting inspections to ensure compliance with radiation protection standards and regulations in industrial and medical facilities.

Mohamed Youssef Messous is a Research Director at National Center for Energy, Sciences and Nuclear Techniques (CNESTEN-Rabat). He was graduated PhD in Physics from the Institute of Nuclear Physics of Lyon-France in 1995. Actually, he is a member of Materials Sciences Unit at CNESTEN. His work is focused on the synthesis and characterisation of materials dedicated for energy conversion and storage, especially photovoltaic and electrochemical energy, and also on radiation detection. In addition to several articles published in indexed journals, he has given courses in different universities and participated in the training of several students (PhDs, Masters, engineers).

Abdessamad Didi is a highly accomplished researcher specialising in nuclear and medical physics, as well as Monte Carlo methods. He has two PhD degrees, one in Materials Science for Energy and Environment from the Faculty of Sciences in Fes, Morocco, and the other in Nuclear Physics from the Faculty of Sciences in Oujda, Morocco. He is working as a researcher the National Centre for Nuclear Energy, Science and Technology in Morocco. His research focuses on spallation physics and its applications in nuclear reactors and medical contexts. He has published extensively in prestigious journals and conferences, primarily in nuclear energy, simulation, and spallation physics. He is an active reviewer and holds editorial roles for various journals, and he has contributed significantly to over 30 international conferences in different committee capacities.

El Mahjoub Chakir is a Professor at Ibn Tofail University, Faculty of Sciences in Kenitra. He earned his PhD in Nuclear Physics from the Faculty of Sciences at Mohammed V University, Rabat, Morocco, in 1994. Currently, he holds the position of Research Professor at the Faculty of Sciences, Ibn Tofail University in Kenitra, Morocco. Additionally, he serves as the Director of the Materials and Subatomic Physics Laboratory at the same institution. His research primarily focuses on reactor physics, medical physics, and science pedagogy. He has a substantial publication record with numerous research articles in indexed international journals, covering both nuclear physics and science pedagogy

El Mehdi Alibrahmi is a Professor and faculty member at Ibn Tofail University, Faculty of Sciences in Kenitra. He has directed numerous scientific research projects in the fields of radiation detection, radioactivity, applied statistics, radiation protection, radiation physics, ionising radiation, environmental

radioactivity, and radiation dosimetry. He has authored many papers and communications in this field and is an Associate Professor at the Higher School of Education and Training.

1 Introduction

Radiation protection stands as a paramount concern across diverse industries and applications where radioactive sources find prevalent use. Be it in agriculture, industry, research, medicine, scientific endeavours, or the operation of nuclear power plants, ensuring the safety of workers, safeguarding the environment, and protecting the general public from the inherent risks of ionising radiation remains an overarching priority (IAEA, 2023). Achieving this delicate balance between reaping the benefits of ionising radiation and averting potential hazards necessitates an unrelenting pursuit of effective radiation protection measures in this pursuit, the development of novel materials boasting superior radiation protection properties is of paramount importance. These materials must exhibit a remarkable capacity for attenuating ionising radiation while accounting for factors spanning the socioeconomic, physical, and mechanical domains. In this ever-evolving landscape of radiation protection, the research community continues to push the boundaries of innovation, seeking materials that not only promise enhanced protection but also align with the practical constraints of a wide array of applications. Concrete, as a foundational construction material, offers a canvas for experimentation and innovation. Its mixtures, tailored to meet specific engineering requirements, provide a versatile platform for the integration of radiation shielding materials (Salem et al., 2023). In this context, our study explores how different concrete compositions, infused with varying barite ores, influence radiation attenuation. This approach, marrying concrete's structural stability with barite's radiation attenuation properties, presents a novel avenue for optimising radiation protection materials (Aygün et al., 2021; El-Samrah et al., 2022; Gunoglu and Akkurt, 2021; Zorla et al., 2017). Barite, a naturally occurring mineral, holds considerable significance in this pursuit. Abundant in Morocco, barite is distinguished by its elevated density, making it a candidate of interest for radiation attenuation (González-Ortega et al., 2015; Sensoy and Gökçe, 2020). Its integration into concrete mixtures introduces the promise of superior radiation shielding properties (Masoud et al., 2020), opening new horizons in the quest for optimised materials in radiation protection applications (Gökçe et al., 2018; Sharifi et al., 2013).

Central to our study is the exploration of how different concrete mixtures, namely Zagora (Zg-a), Agdz (Ag-a), Tijjekht (Tj-a), Ras Kammouna (Rk-a), and Tinejdad (Tnj-a), will respond when exposed to irradiation from commonly encountered radioactive sources such as ^{60}Co, ^{133}Ba, and ^{137}Cs. To achieve this, a multifaceted approach is adopted, seamlessly merging computational simulations with experimental validation techniques. In this study, the Monte Carlo N-Particle (MCNP) code plays a central role in predicting photon behaviour within diverse concrete mixtures, owing to its robust reputation in radiation transport simulations. Additionally, calculations using DOSIMEX and XCOM codes provide supplementary insights into the radiation protection attributes of these concrete materials. To ensure the credibility of our theoretical calculations obtained through the MCNP and DOSIMEX codes, as well as

XCOM, rigorous experimental measurements, are used to anchor our findings in empirical evidence.

The innovation encapsulated within these novel concrete mixtures opens up a vista of opportunities for radiation shielding across activities involving radioactive isotopes characterised by neutron, γ, and X-ray emissions. The practical applications are manifold, encompassing domains such as prompt gamma activation analysis (PGAA) (Amsil et al., 2023), experiment calibration, laboratory partition construction, and the secure immobilisation and containment of radioactive waste (El Azzaoui et al., 2022). Importantly, given Morocco's standing as the world's third-largest producer of barite, the results of this study hold the potential for widespread adoption, offering a readily deployable solution in the realm of radiation protection.

2 Materials and methods

2.1 Materials

As stated in the introduction section, this study delves into the attenuation characteristics of barite extracted from five distinct ore sites as presented in Figure 1: Zg-a, Ag-a, Tj-a, Rk-a, and Tnj-a. We have meticulously crafted four unique formulations for each mine site, systematically varying the percentage of barite content across a range from 6% to 69%. Table 1 provides a comprehensive breakdown of the constituents and their corresponding proportions within these formulations, offering a clear overview of the configurations of concrete samples. Each sample embeds barite sourced from specific mine sites. Within each mine site category, we have diligently prepared four distinct formulations, labelled M1, M2, M3, and M4. Each formulation features a precise percentage of barite derived from the respective mine site. We have explicitly delineated the specific ingredients and their proportional contributions for each formulation, shedding light on the exact composition of the samples under our scrutiny.

To quantify the residual water content within the samples following solidification (after 28 days), we monitored the evaporation percentage over a specific timeframe, as delineated in Table 2. This table comprehensively also displays the water percentage concerning the sample weight across our M1, M2, M3, and M4 mixtures. These percentages were found to be 3.35%, 3.83%, 4.31%, and 4.78%, respectively. It's important to note that our simulation considered only the water that remained in the samples after solidification and did not account for the initial quantity of water used during the sample preparation process.

Table 1 Composition of mixtures

	Cement (%)	*Barite (%)*	*Sand (%)*	*Water (%)*
M1	16	6	71	7
M2	16	21	55	8
M3	16	42	33	9
M4	16	69	5	10

Concerning the components comprising the concrete under scrutiny in this study, they predominantly consist of Portland cement CPJ45 (Naamane et al., 2016), barite extracted from the five specified sites (Essalhi et al., 2018), and sand sourced from Mir left (Laasri

et al., 2016). To ascertain the elemental composition in terms of oxides, we employ the molar mass of the individual elements as presented in Table 3. This approach enables the determination of the weight or mass percentage corresponding to each element within the oxides. This calculation conventionally relies on the atomic composition inherent in the compounds.

Figure 1 Moroccan map, showing the positions of the studied mine sites in the Daraa-Tafilalt region (see online version for colours)

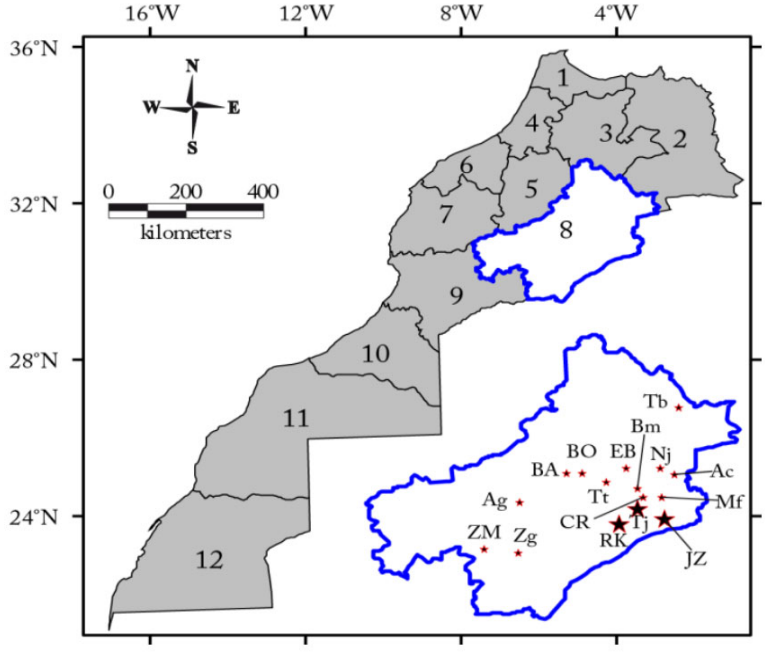

Source: Essalhi et al. (2018)

Table 2 Percentage of evaporation monitoring compared to initial water weight in samples over time

Time (hours)	*2*	*4*	*8*	*24*	*28*	*32*	*37*	*672 (28 days)*
Water evaporation percentage (%)	7.89	12.33	17.78	30.11	34.56	36.78	41.22	47.89

The characteristics of the radioactive sources utilised in this study are presented in Table 4. The choice of these three sources is validated by their widespread utilisation in various applications and domains. Moreover, their emission spectrum encompasses both high and medium-energy emissions, exemplified by energies such as 1.33 MeV (99.98%), 1.17 MeV (99.97%), 0.66 MeV (85.10%), and 0.35 MeV (62.05%).

2.2 Methods

In our study, we employed a combination of simulation tools and experimental measurements to validate our theoretical calculations. To conduct simulations, we utilised three key codes: MCNP, DOSIMEX, and XCOM.

Table 3 Chemical composition of ingredients in the sample formulations

Chemical element	*Atomic number (Z)*	*Barite Zg-a (Wt. %)*	*Barite Ag-a (Wt. %)*	*Barite Tj-a (Wt. %)*	*BariteRk-a (Wt. %)*	*Barite Tnj-a (Wt. %)*	*Cement CPJ45 (Wt. %)*	*Sand (Wt. %)*	*Water (Wt. %)*
H	1	-	-	-	-	-	-	-	11.190
O	8	27.553	27.553	27.979	28.644	27.626	32.144	36.040	88.790
Na	11	-	-	-	-	-	0.130	-	-
Mg	12	0.012	0.006	0.012	0.024	-	0.650	0.740	-
Al	13	0.058	0.106	0.074	0.185	0.064	2.170	3.390	-
Si	14	-	0.051	0.673	2.188	0.290	8.860	22.620	-
P	15	-	-	-	-	-	0.030	0.040	-
S	16	13.752	13.716	13.453	12.623	13.626	1.230	-	-
K	19	-	0.008	0.008	0.108	0.008	0.680	1.430	-
Ca	20	0.021	0.021	0.050	0.550	0.021	42.350	14.25	-
Ti	22	-	-	-	-	-	-	0.096	-
Mn	25	-	-	-	-	-	-	0.015	-
Fe	26	0.007	0.027	0.622	1.245	0.077	1.700	1.550	-
Sr	38	1.383	0.801	1.727	0.954	1.092	-	-	-
Ba	56	56.728	57.487	54.910	52.568	56.646	-	-	-

Source: Essalhi et al. (2018)

Table 4 Characteristics of used radioactive sources in this work

Radionuclide	*Half-live (year)*	*Photon energy (MeV)*	*Photon intensity (%)*	*Residual activity (KBq)*
^{60}Co	5.27	1.173237 (γ)	99.97	210
		1.332501 (γ)	99.98	
^{137}Cs	30.08	0.661657 (γ)	85.10	740
		0.004466 (X)	0.36	
		0.004827 (X)	0.22	
		0.031817 (X)	2.04	
		0.032194 (X)	3.76	
		0.036378 (X)	0.68	
		0.037255 (X)	0.21	

Source: Chu et al. (1999)

Table 4 Characteristics of used radioactive sources in this work (continued)

Radionuclide	*Half-live (year)*	*Photon energy (MeV)*	*Photon intensity (%)*	*Residual activity (KBq)*
^{133}Ba	10.50	0.080997 (γ)	34.06	440
		0.276398 (γ)	7.16	
		0.302853 (γ)	18.33	
		0.356017 (γ)	62.05	
		0.383851 (γ)	8.94	
		0.004286 (X)	6.00	
		0.004620 (X)	3.80	
		0.030625 (X)	34.90	
		0.030973 (X)	64.50	
		0.034920 (X)	5.99	
		0.034987 (X)	11.60	
		0.035818 (X)	3.58	

Source: Chu et al. (1999)

2.2.1 MCNP code

The MCNP code, originally developed at the Los Alamos National Laboratory, serves as a versatile tool designed to track a wide spectrum of particles, including neutrons, electrons, photons, and more, across a broad energy range (Werner, 2017). In our research, we harnessed MCNP to simulate various radiation protection parameters of our prepared samples. These parameters encompassed linear attenuation coefficients (LAC or μ), mass attenuation coefficients (μ/ρ), radiation protection efficiency (RPE), and half-Value Attenuations (HVL). In our case, we used the F4 tally to calculate the fluence, which was then multiplied by the conversion coefficient to obtain the dose rate.

2.2.2 DOSIMEX code

The DOSIMEX code was employed to calculate the dose equivalent rates of beta (β), γ, and X-rays emanating from ionising radiation sources. This code operates on deterministic principles and incorporates attenuation calculations in straight lines, along with build-up correction methods (Vivier and Lopez, 2019).

2.2.3 XCOM

XCOM is a widely recognised computational tool in the fields of radiation physics and material science. XCOM provides comprehensive data concerning the interaction of photons with various materials, offering valuable insights into attenuation and scattering behaviours. Researchers benefit from the accurate and reliable information available through XCOM, aiding in the design and analysis of radiation-shielding materials. Its extensive database spans a wide energy range, making it an indispensable resource for the study of radiation-matter interactions and the optimisation of radiation protection strategies (NIST, 2010).

Figure 2 Schematic picture, (a) theoretical and experimental configuration, employing proportional detector and isotropic sources (b) the generated geometry by MCNP (see online version for colours)

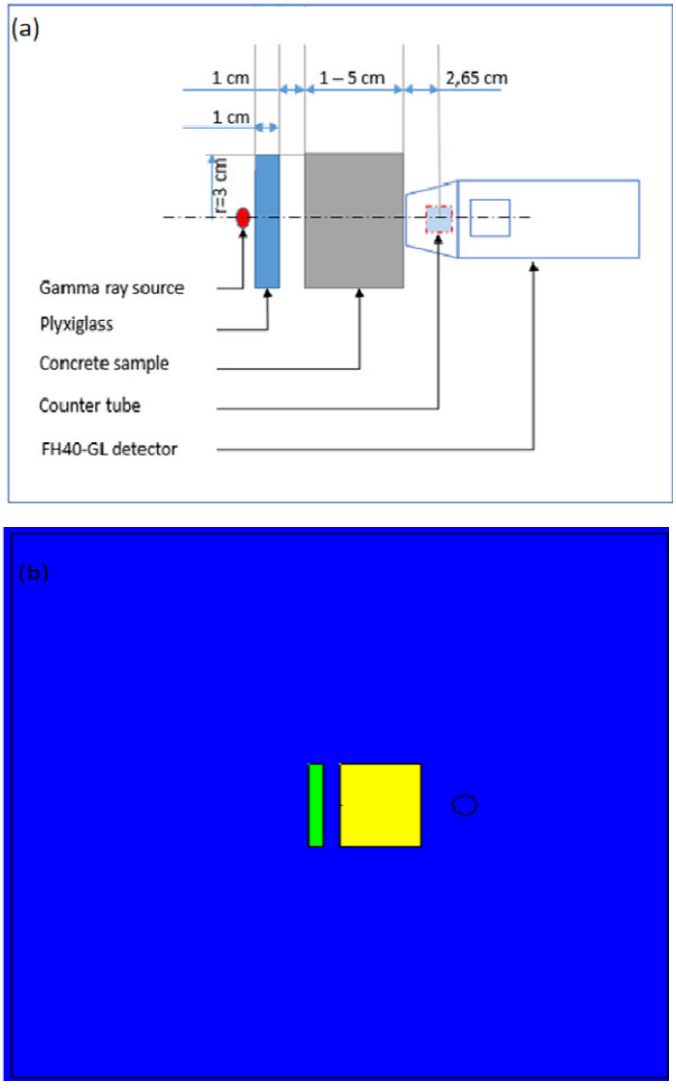

By harnessing the capabilities of MCNP, DOSIMEX, and XCOM, our research gained valuable tools for comprehending and analysing radiation protection measures. These codes facilitated our assessment and optimisation of the shielding properties of materials while allowing us to evaluate potential risks associated with ionising radiation sources. To provide a visual representation of our setups, Figures 2 and 3 vividly illustrate the 2D and 3D configurations, enhancing the clarity of our experimental arrangements.

Figure 3 Schematic of 3-D simulation (see online version for colours)

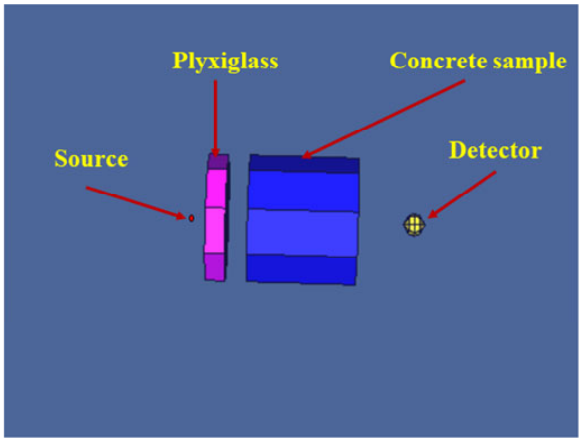

2.2.4 Experimental configuration

In our pursuit of experimental measurements, we employed the FH40 G-L10 digital proportional counter gas tube detector, a sophisticated instrument manufactured by Thermo Scientific. This apparatus allowed us to precisely quantify the ambient dose equivalent rate (H*(10)) for γ and X-rays, spanning energies from 0.03 MeV to 4.40 MeV (APVL, 2023). To ensure the reliability of our experimental data, we conducted ten measurements and computed their average.

For consistency in assessing the identical physical quantity, H*(10), we utilised Integration coefficients (ICRU), establishing a critical connection between photon fluence and ambient dose (ICRU, 2020). These conversion coefficients played a pivotal role in bridging the gap between protection and operational quantities, facilitating a comprehensive evaluation of our measurements.

In terms of mitigating β-radiation, commonly used materials include Plexiglas, glass, and aluminium. To align our simulations with experimental conditions, we introduced a 1 cm layer of Plexiglas as shielding against β-radiation. This thickness effectively shields against all β-rays with energies equal to or less than 2 MeV (Métivier, 2002). Given that the energies of Beta particles emitted by radioelements like ^{60}Co, ^{133}Ba, and ^{137}Cs fall below 2 MeV, our analysis concentrated specifically on γ and X-ray radiations.

2.2.5 Theoretical aspect

To calculate the linear attenuation coefficient (LAC) the following standard equation (Beer-Lambert law) was used (Métivier, 2002; Nassreldeen and Elsheikh, 2020):

$$I = I_0 . B . e^{-\mu x} \tag{1}$$

In the context of the equation, μ represents the LAC of the material, expressed in cm^{-1}. The variable x pertains to the thickness of the absorber, while I and I0 denote the counts of γ-rays per second, with and without the shielding material, respectively. The factor denoted as B corresponds to the Build-up factor. The Mass attenuation coefficients were calculated by using this equation (2) (Sensoy and Gökçe, 2020).

$$\mu_m = \mu / \rho \tag{2}$$

where μ_m: mass attenuation coefficient (cm^2/g), μ: linear attenuation coefficient (cm^{-1}), and ρ: concrete density (g/cm^3).

On the other hand, the HVL signifies the absorber thickness that diminishes the initial radiation level by a factor of 2. The computation of HVL is governed by the subsequent equation (Biswas et al., 2016).

$$HVL = \frac{Ln(2)}{\mu} = \frac{0.693}{\mu} \tag{3}$$

The latter equation is derived from equation (1) without accounting for the build-up effect. Within the context of the radiation protection criteria, the RPE takes on a significant role. It serves as an additional parameter of essential importance, serving to gauge the effectiveness of our concrete shielding. Its primary function lies in assessing how effectively the shielding prevents the penetration of photons. The RPE provides a quantifiable measure, essentially quantifying the number of attenuated photons by the concrete sample. The determination of a material's RPE at a particular energy is conducted as follows (Sharma et al., 2020):

$$RPE = \left(1 - \frac{I}{I_0}\right) * 100 \tag{4}$$

3 Results and discussion

Figure 4 shows XCOM data that vividly depicts dynamic shifts in the LAC across five meticulously prepared samples. These samples contain 69% barite from different ore sites: Zagora (Zg-a), Agdz (Ag-a), Tijjekht (Tj-a), Ras Kammouna (Rk-a), and Tinejdad (Tnj-a), with densities 3.47g/cm^3, 3.49 g/cm^3, 3.43 g/cm^3, 3.39 g/cm^3, 3.46 g/cm^3, respectively. We also use ordinary concrete (OB) with a density of 3.35 g/cm^3 as a reference point (Jr et al., 2011) Notably, the value of LAC is intricately responsive to both photon energy and the nature of the shielding material (Hernandez-Murillo et al., 2020). To establish a definitive benchmark, we measured the LAC from 0.15 MeV to 1.50 MeV. The findings highlight a direct relationship between the values observed in the formulations under consideration and the concurrent increase in barite concentration and photon energy. The Agdz ore site is noteworthy for having the highest barite concentration (57.48% by weight) and exhibiting the most prominent attenuation characteristics. Moreover, Figure 4 clearly shows a discernible difference in attenuation properties between standard concrete and barite-enriched mixtures. This divergence decreases noticeably as energy levels increase, implying that barite-laden formulations are more effective, especially at lower energy levels. At energy levels of 0.15 MeV, 0.3 MeV, 0.6 MeV, 0.8 MeV, 1 MeV, and 1.25 MeV, significant attenuation differentials of approximately 77%, 48%, 30%, 30%, 29%, and 28% are observed, respectively.

Concerning the findings depicted in Figure 5, our analysis is centred around four distinct formulations – M1, M2, M3, and M4 – where each formulation exclusively integrates barite sourced from the Agdz ore site. The core objective of these results is to

validate the enhancement in shielding efficacy that corresponds to the gradual escalation of barite percentage within the material.

Figure 4 Comparison of LAC for mixtures containing 69% barite from five ore sites and ordinary concrete, using XCOM data (see online version for colours)

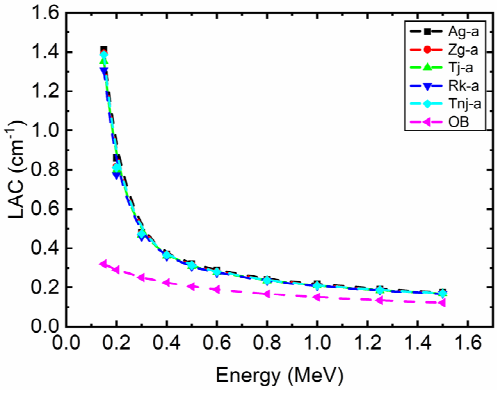

This advancement can be attributed to the heightened prevalence of interactions facilitated by the photoelectric effect, a factor that holds noteworthy significance in the realm of radioprotection.

Figure 5 Comparison of the LAC of four mixtures with varying percentages of Agdz ore site barite, using XCOM data (see online version for colours)

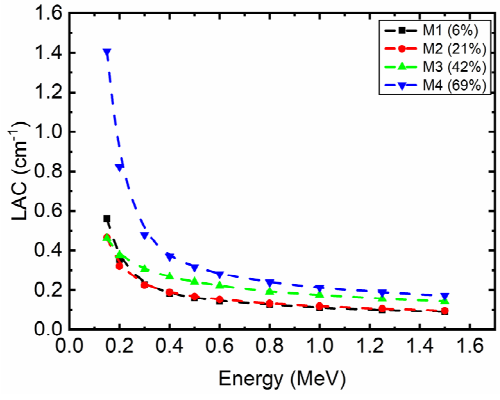

Concerning the RPE, Figure 6 presents the computed RPE values for the five distinct ore sites. This evaluation encompasses both the initial and transmitted photons, ensuring a comprehensive assessment. A close look at the RPE graph reveals a discernible pattern: a striking trend of remarkable attenuation capabilities emerges within the concrete formulation M4, enriched with a 69% barite concentration. This phenomenon is especially noticeable at higher energies, specifically at 1.173 MeV and 1.332 MeV. Remarkably, the zenith of RPE among the rigorously prepared ore sites attains an impressive 45.97%, aligning precisely with the Agdz site (Ag-a). In stark contrast, standard concrete achieves a modest RPE of only 32.84%. This glaring contrast underscores the pivotal role played by barite within our formulation, reinforcing its

essential contribution to effectively mitigating the impact of γand X rays radiation originating from photons.

Figure 6 Comparing the RPE coefficients across the five distinct ore sites using a shielding thickness of 5 cm (see online version for colours)

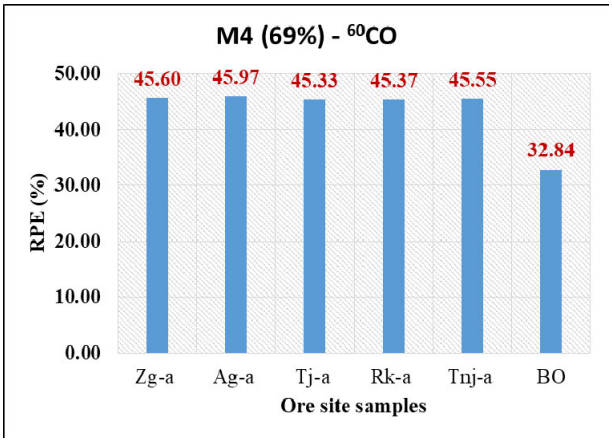

Figure 7 Dose rate H*(10) variation in mixture M4 with Agdz ore site barite, under ^{60}Co irradiation, as a function of thickness (see online version for colours)

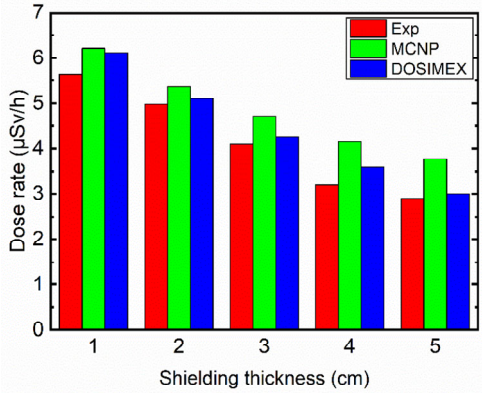

Figure 7, Figure 8, and Figure 9 provide visual representations of the dynamic trends in experimental (Exp) dose rates (H*(10)), meticulously measured by the FH40 G-L10 dose rate meter. Moreover, these figures contrast these measured values with the simulated outcomes yielded by MCNP and DOSIMEX computations. These assessments were conducted on the Ag-a sample, containing 69% barite as our shielding, which exhibits notable attenuation characteristics for both γ and X-rays. The dose rate was investigated across varying thicknesses, ranging from 1 to 5 cm, for different radioelements ^{60}Co, ^{137}Cs, and ^{133}Ba. Furthermore, upon scrutinising Figure 7, Figure 8, and Figure 9, a consistent pattern unfurls across the spectrum from 1 cm to 5 cm. Notably, both experimental and simulated outcomes – captured by both MCNP and DOSIMEX data – resonate well. It's worth noting, however, that the specific configuration employed in this study results in a relatively subdued build-up factor (Vivier and Lopez, 2021). As

a consequence, the DOSIMEX calculations stand unencumbered by the build-up effect. The attenuation factor in dose, calculated as the ratio of the dose rate with shielding to the dose rate without shielding, registers at 1.85, 2.57, and 6.83 for radioelements ^{133}Ba, ^{137}Cs, and ^{60}Co respectively, utilising 5 cm of the examined mixture. This signifies a robust attenuation capability of our mixture against photons. Importantly, the efficiency of our mixture appears to heighten as energy levels decrease.

Figure 8 Dose rate H*(10) variation in mixture M4 with Agdz ore site barite, under ^{137}Cs irradiation, as a function of thickness (see online version for colours)

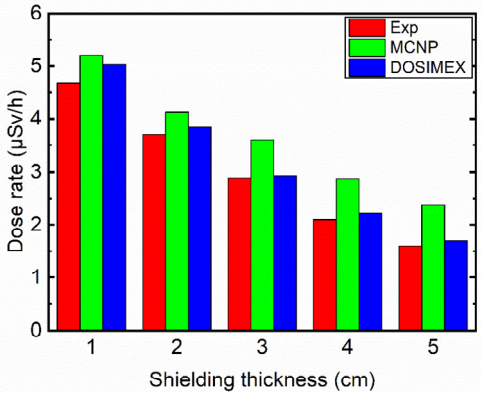

Figure 9 Dose rate H*(10) variation in mixture M4 with Agdz ore site barite, under ^{133}Ba irradiation, as a function of thickness (see online version for colours)

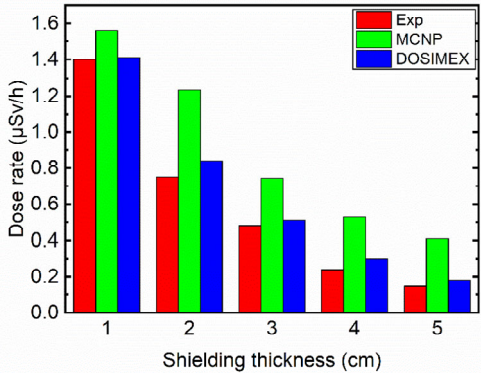

The half-value layer HVL represents the precise thickness of the attenuator required to halve the original photon intensity. This parameter is inversely proportional to the density of the sample. Figure 10 presents data concerning the HVL for the prepared concrete mixtures, including varying percentages of barite, as well as ordinary concrete. Notably, as the photon energy shifts within the range of 0.15 MeV to 1.50 MeV, the HVL values exhibit an increasing trend. This observation implies that higher photon energies enhance their capacity to penetrate the investigated concrete compositions. Furthermore, the outcomes of the analysis reveal that the HVL for the concrete sample with the highest barite density, Ag-a (57.48%), is comparatively lower than that of other mixtures—Zg-a (56.72%), Tj-a (54.91%), Rk-a (52.56%), and Tnj-a (56.64%). Particularly, the mixture

Rk-a (52.56%), characterised by the lowest barium weight fraction, showcases the highest HVL values. The graph prominently illustrates that ordinary concrete manifests the highest HVL when contrasted with formulations incorporating barium. These findings offer valuable insights into the role of barium in radiation shielding.

Figure 10 Comparison of half value layer (HVL) for the prepared concretes in energy region between 0.15 MeV and 1.50 MeV (see online version for colours)

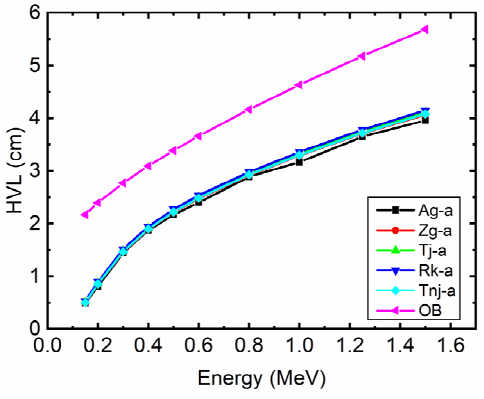

Figure 11 Calculated mass attenuation coefficients as a function of photon energy for the mixture containing 69% of the barite from the Agdz ore site

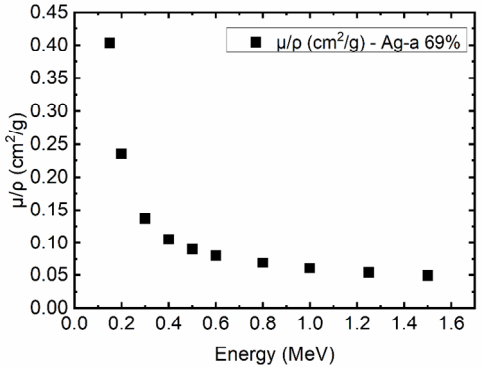

Figure 11 provides a graphical representation of the interplay between mass attenuation coefficients and photon energy, spanning the energy range of 0.15 MeV to 1.50 MeV. The primary focus centres on the formulation that exhibits the highest attenuation coefficient, notably comprising 69% barite sourced from the Agdz ore site. The data illustrated in the figure is derived from XCOM calculations. The graph distinctly reveals the trend of μ/ρ decreasing significantly with energy. This signifies that the prepared sample, characterised by Agdz ore site barite at 69%, excels in attenuation capability at lower energies, but this capability diminishes as energy levels rise.

The distinct average energies of ^{60}Co and ^{137}Cs, at 1.25 MeV and 0.6 MeV respectively, pave the way for the determination of specific mass attenuation coefficients. Figure 12 offers a comprehensive comparison of these coefficients pertinent to our mixture concerning both ^{60}Co and ^{137}Cs. This comparison amalgamates data from

experimental, MCNP, DOSIMEX, and XCOM sources. Upon careful analysis of the figure, a striking convergence among the acquired outcomes becomes apparent. This alignment underscores a robust agreement between the applied theoretical models and the empirical findings.

Figure 12 Mass attenuation coefficients obtained by experimental, MCNP, DOSIMEX, and XCOM for prepared sample (Ag-a (69%)) with the variation of radioelements (see online version for colours)

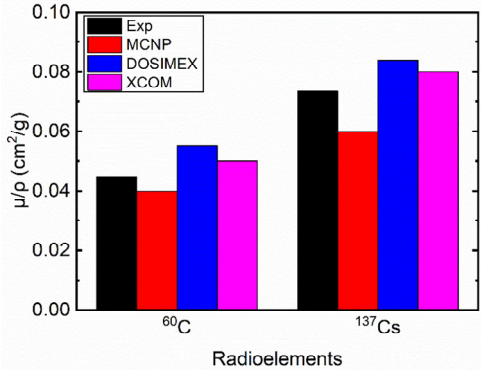

4 Conclusions

The core objective of this study was to comprehensively evaluate and present MCNP, DOSIMEX, and XCOM and experimental outcomes about the attenuation characteristics of γ and X-rays within concrete formulations incorporating barite from five distinct ore sites, covering a spectrum of energy levels. The principal conclusions derived from this endeavor are outlined as follows:

- The formulation yielding the most robust radiation protection properties concerning γ and X-ray attenuation is the composition (M4/Ag-a), which entails 16% cement, 69% barite sourced from the Agdz ore site, 5% sand, and 10% water.
- The Agdz ore site, featuring 57.48% barite content, emerges as the pinnacle of radiation protection efficacy.
- The differential between the developed mixtures and conventional concrete registers at approximately 54% in terms of their attenuation capabilities.
- Encouragingly, the experimental data garnered demonstrate a commendable alignment with the theoretical calculations as furnished by MCNP, DOSIMEX, and XCOM.

These discernible findings underscore the exceptional efficacy of the devised mixtures in augmenting radiation protection characteristics, thereby underscoring the pivotal role played by barite content in heightening attenuation properties. The congruence between empirical and simulation results underscores the validity of computational tools in evaluating radiation shielding attributes. Future perspectives for this research will encompass a spectrum of work, such as the validation of results using alternative

simulation codes to ensure the robustness of the findings. Furthermore, there is ample opportunity to investigate shielding properties under the combined influence of both neutron and gamma spectrums, a feature that is critical in practical applications. Furthermore, investigating other concrete mixtures containing enriched barite could provide insights into a broader range of radiation protection materials, contributing to the advancement of radiation shielding solutions.

References

Amsil, H., didi, A., Bounouira, H., Aarab, I., Badague, A., Laraki, K., Jalil, A., Elmokhtari, B., Elamri, L. and Kabach, O. (2023) 'The Moroccan PGAA system: design, installation, and challenges', *Arab J. Nucl. Sci. Appl.*, Vol. 56, pp.39–48, https://doi.org/10.21608/ajnsa.2022.174753.1685.

APVL (2023) *Gamme de radiamètres FH 40 G Caractéristiques techniques*, Saint-Cyr-sur-Loire.

Aygün, B., Şakar, E., Agar, O., Sayyed, M.I., Karabulut, A. and Singh, V.P. (2021) 'Development of new heavy concretes containing chrome-ore for nuclear radiation shielding applications', *Prog. Nucl. Energy*, p.133, https://doi.org/10.1016/j.pnucene.2021.103645.

Biswas, R., Sahadath, H., Mollah, A.S. and Huq, M.F. (2016) 'Calculation of gamma-ray attenuation parameters for locally developed shielding material: Polyboron', *J. Radiat. Res. Appl. Sci.*, Vol. 9, pp.26–34, https://doi.org/10.1016/j.jrras.2015.08.005.

Chu, S.Y.F., Ekström, L.P. and Firestone, R.B. (1999) *The Lund/LBNL Nuclear Data Search – Version 2.0*, February [online] http://nucleardata.nuclear.lu.se/toi/index.asp (accessed 29 April 1998).

El Azzaoui, B., Hamdane, H., Outayad, R., Mimount, S., El Ghailassi, T., Elabbari, Y., Chakir, E.A. and Alibrahmi, E.M. (2022) 'Non-destructive techniques as a tool for radioactive waste package performance testing in order to ensure long-term safety', *SSRN Electron. J.*, Vol. 14, pp.1425–1434, https://doi.org/10.2139/ssrn.4188600.

El-Samrah, M.G., Abreu Zamora, M.A., Novog, D.R. and Chidiac, S.E. (2022) 'Radiation shielding properties of modified concrete mixes and their suitability in dry storage cask', *Prog. Nucl. Energy*, Vol. 148, p.104195, https://doi.org/10.1016/j.pnucene.2022.104195.

Essalhi, M., Mrani, D., Essalhi, A., Toummite, A. and Ali-Ammar, H. (2018) 'Evidence of a high quality barite in Drâa-Tafilalet region, Morocco: a non- upgraded potential', *J. Mater. Environ. Sci.*, Vol. 9, pp.1366–1378, https://doi.org/doi.org/10.26872/jmes.2017.9.4.149.

Gökçe, H.S., Yalçınkaya, Ç. and Tuyan, M. (2018) 'Optimization of reactive powder concrete by means of barite aggregate for both neutrons and gamma rays', *Constr. Build. Mater.*, Vol. 189, pp.470–477, https://doi.org/10.1016/j.conbuildmat.2018.09.022.

González-Ortega, M.A., Cavalaro, S.H.P. and Aguado, A. (2015) 'Influence of barite aggregate friability on mixing process and mechanical properties of concrete', *Constr. Build. Mater.*, Vol. 74, pp.169–175, https://doi.org/10.1016/j.conbuildmat.2014.10.040.

Gunoglu, K. and Akkurt, İ. (2021) 'Radiation shielding properties of concrete containing magnetite', *Prog. Nucl. Energy*, p.137, https://doi.org/10.1016/j.pnucene.2021.103776.

Hernandez-Murillo, C.G., Molina Contreras, J.R., Escalera-Velasco, L.A., de Leon-Martínez, H.A., Rodriguez-Rodriguez, J.A. and Vega-Carrillo, H.R. (2020) 'X-ray and gamma ray shielding behavior of concrete blocks', *Nucl. Eng. Technol.*, Vol. 52, pp.1792–1797, https://doi.org/10.1016/j.net.2020.01.007.

IAEA (2023) *Radiation Protection and Radioactive Waste Management in the Design and Operation of Research Reactors*, August, p.202, ISSN 1020–525X ; no. SSG-85, IAEA Library, Austria.

ICRU (2020) 'Appendix A. Values of conversion coefficients', *J. ICRU.*, https://doi.org/10.1177/1473669120966219.

Jr, R.M., Gesh, C., Pagh R., Rucker, R. and Williams III, R.G. (2011) *Compendium of Material Composition Data for Radiation Transport Modeling Report*, Richland, Washington, University of North Texas Libraries, UNT Digital Library.

Laasri, A., Et-taleb, S., Morad, Y., Hilali, M. and Benlhachemi, A. (2016) 'Physico-chemical study of marine waters sands in the region of Sidi Ifni: Particle size and determination of the concentration of heavy metals', *J. Mater. Environ. Sci.*, Vol. 7, No. 12, pp.4778–4785.

Masoud, M.A., Kansouh, W.A., Shahien, M.G., Sakr, K., Rashad, A.M. and Zayed, A.M. (2020) 'An experimental investigation on the effects of barite/hematite on the radiation shielding properties of serpentine concretes', *Prog. Nucl. Energy*, Vol. 120, p.103220, https://doi.org/10.1016/j.pnucene.2019.103220.

Métivier, C.J.H. (2002) 'La personne compétente en radioprotection', *Revue Générale Nucléaire*, https://doi.org/10.1051/rgn/20022067.

Naamane, S., Rais, Z. and Taleb, M. (2016) 'The effectiveness of the incineration of sewage sludge on the evolution of physicochemical and mechanical properties of Portland cement', *Constr. Build. Mater.*, Vol. 112, pp.783–789, https://doi.org/10.1016/j.conbuildmat.2016.02.121.

Nassreldeen, A. and Elsheikh, A. (2020) 'Gamma-ray and neutron shielding features for some fast neutron moderators of interest in 252Cf-based boron neutron capture therapy', *Appl. Radiat. Isot.*, Vol. 156, p.109012, https://doi.org/10.1016/j.apradiso.2019.109012.

NIST (2010) *XCOM: Photon Cross Sections Database*, https://doi.org/https://dx.doi.org/10.18434/T48G6X.

Salem, M.M., Kenawy, E-R., Zakaly, H.M.H., Ene, A., Azaam, M.M., Edries, T.B., Zhou, D., Hussein, M.M., Abd El-Hameed, A.S., Nabil, I.M. and Darwish, M.A. (2023) 'Electrospun PVDF/Barium hexaferrite fiber composites for enhanced electromagnetic shielding in the X-band range', *Results Phys.*, Vol. 53, p.106975, https://doi.org/10.1016/j.rinp.2023.106975.

Sensoy, A.T. and Gökçe, H.S. (2020) 'Simulation and optimization of gamma-ray linear attenuation coefficients of barite concrete shields', *Constr. Build. Mater.*, Vol. 253, p.8, https://doi.org/10.1016/j.conbuildmat.2020.119218.

Sharifi, S., Bagheri, R. and Shirmardi, S.P. (2013) 'Comparison of shielding properties for ordinary, barite, serpentine and steel-magnetite concretes using MCNP-4C code and available experimental results', *Ann. Nucl. Energy*, Vol. 53, pp.529–534, https://doi.org/10.1016/j.anucene.2012.09.015.

Sharma, A., Sayyed, M.I., Agar, O., Kaçal, M.R., Polat, H. and Akman, F. (2020) 'Photon-shielding performance of bismuth oxychloride-filled polyester concretes', *Mater. Chem. Phys.*, Vol. 241, p.122330, https://doi.org/10.1016/j.matchemphys.2019.122330.

Vivier, A. and Lopez, G. (2019) *Code de calcul de dose - gamma - manuel d'utilisation - DOSIMEX - GX 3.0*.

Vivier, A. and Lopez, G. (2021) *Dossier de validation emission gamma (radionucleides) DOSIMEX-GX 3.1*.

Werner, C.J. (2017) *MCNP User's Manual Code Version 6.2*, Los Alamos National Laboratory, LA-UR-17-29981.

Zorla, E., Ipbüker, C., Biland, A., Kiisk, M., Kovaljov, S., Tkaczyk, A.H. and Gulik, V. (2017) 'Radiation shielding properties of high performance concrete reinforced with basalt fibers infused with natural and enriched boron', *Nucl. Eng. Des.*, Vol. 313, pp.306–318, https://doi.org/10.1016/j.nucengdes.2016.12.029.